PLASMA TURBULENCE

Plasma occurs in states of turbulence under a wide range of conditions including space and astrophysical plasmas as well as those produced in laboratory confinement devices. The strength of the turbulence increases as the plasma is driven

further away from thermodynamic equilibrium. While there are many ways to drive the plasma away from equilibrium with particle beams, laser beams, and radio-frequency waves, the universally occurring departures from equilibrium considered here are (1) the presence of plasma currents and (2) the existence of spatial gradients. While both driving forces may exist simultaneously, it is sufficient to consider the effects independently here.

In the section entitled "Current-Driven Turbulence" we describe the types of plasma turbulence that occur in the uniform plasma in which the role of magnetic fields is negligible on the fast ion acoustic wave turbulence and the Buneman instability driven by a current density $j = -enu$ (A/m^2) in a plasma. Here n is the plasma density and u the relative drift velocity of the electrons with respect to the ions. The electron charge is $-e$ and mass is m_e. The plasma turbulence provides the mechanism for the exchange of energy and momentum between the electrons and ions. The turbulence determines the current–voltage relationship through the anomalous resistivity $\eta = m_e\nu_{\text{eff}}/ne^2$ where ν_{eff} is the rate of change of the electron momentum $m_e\boldsymbol{u}$, measured relative to the ion rest frame, due to the turbulent electric fields. The energy density in the turbulence is W (J/m^3). The dependence of ν_{eff} on u/v_e for both regimes is shown in Fig. 1. Experiments have confirmed the general features of the small fraction turbulence level W/n_eT_e producing a substantial anomalous resistivity $\nu_{\text{eff}}/\omega_{pe} \lesssim 0.2(m_e/m_i)^{1/3}$ and a fast turbulent heating of the electrons. Once the electron temperature T_e increases to the value such that the associated thermal velocity $v_e = (k_BT_e/m_e)^{1/2} > 2u$, the turbulence enters a weaker regime where $\nu_{\text{eff}} \simeq \omega_{pe}(u/v_e)(T_e/T_i) \times 10^{-3}$. The dependence of ν_{eff} on the drift velocity u makes Ohm's law, $E = \eta j = (m_e\nu_{\text{eff}}/ne^2)j$, nonlinear. There is substantial plasma heating and the production of a fast ion tail on the ion distribution in the ion acoustic turbulence phase of the experiments.

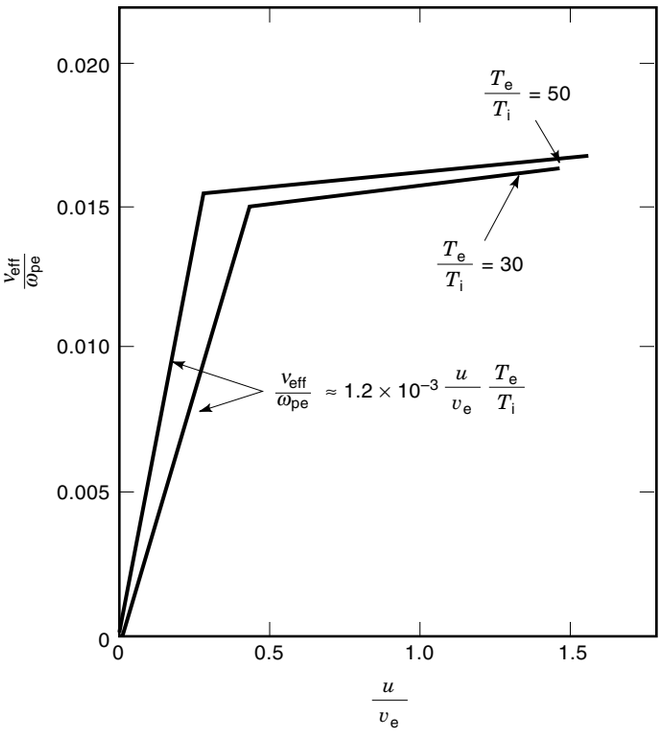

Figure 1. The dependence of the effective electron collision frequency ν_{eff} on the drift velocity of the electrons with respect to the ions. The regime of $u/v_e \lesssim 0.5$ is dominated by ion acoustic turbulence while the regime of $u/v_e \gtrsim 1$ is that of the two-stream instability.

In the section entitled "Spatial Gradient-Driven Turbulence in Magnetized Plasma" the case of plasma turbulence produced by the spatial gradients from its confinement. The confinement or trapping of a plasma is produced both in the laboratory and in space/astrophysics by magnetic fields that cause the charged particles to gyrate with radius $\rho_a = m_av_a/q_aB$ around the local magnetic field $\boldsymbol{B}(\boldsymbol{x})$. The confinement along $\boldsymbol{B}$ (parallel to $\boldsymbol{B}$) occurs either due to the large increase of $|B|$ giving rise to the mirror effect as in Earth's magnetosphere or due to the field lines forming closed, nested toroidal surfaces as in solar current loops and the laboratory tokamak device. From over 30 years of laboratory research in the tokamak confinement studies of plasma, there is a detailed understanding of the intrinsic, irreducible plasma turbulence that develops from spatial gradients. This turbulence is generically called drift wave turbulence and is driven by the cross-field gradients of the plasma density $\nabla n = -(n/L_n)\hat{\boldsymbol{e}}_x$ and temperature $\nabla T = -(T/L_T)\hat{\boldsymbol{e}}_x$. While there are many detailed forms known for the turbulence depending on the plasma parameters, there are essentially three generic results for the plasma cross-field diffusivities D (m^2/s) of particles and χ (m^2/s) for thermal diffusivity. The three functionally distinct forms are: (1) the Bohm diffusivity $D_B = \alpha_B(T_e/eB)$, (2) the gyro-Bohm diffusivity from drift waves $D_{dw} = \alpha_{dw}(\rho_i/L_T)(T_e/eB)$, where $\rho_i = (m_iT_i)^{1/2}/eB$ is the thermal ion gyroradius, and the (3) collisional turbulence diffusivities $D_r = \alpha_{rg}\nu_e\rho_e^2(L_s^2/L_TR_c)$ where ν_e is electron–ion collision frequency associated with resistivity $E_\parallel = \eta j_\parallel$ along the magnetic field. The Bohm diffusivity varies as T/B and is documented in Taroni et al. (1) and Erba et al. (2), for the tokamak with a low coefficient $\alpha_B \sim \frac{1}{200}$. The drift wave transport varies as $T^{3/2}/B^2L$ and is documented in Horton (3) with a coefficient $\alpha_{dw} \sim 0.3$ (4). The resistive interchange mode diffusivity varies as $\chi_{rg} \sim n/T_e^{1/2}B^2$ and has a coefficient of order unity (5). The coefficients α_B, α_{dw}, and α_{rg} are weak functions of many detailed plasma parameters such T_e/T_i, L_T/R, $\beta = 2\mu_0p/B^2$, and more. Just as in neutral fluid turbulence, there are many degrees of freedom excited in plasma turbulence and there is great difficulty in determining the details of these formulas either through theory or numerical simulations. Nonetheless, the years of experience with the tokamak program have led to rather firm general conclusions about the turbulent diffusivities. The study of the boundary layers between different types of plasmas in the magnetosphere have also shed light on the limits of the collisionless plasma transport rates.

Now we present some details of these two fundamental forms of plasma turbulence.

CURRENT-DRIVEN TURBULENCE

Large currents naturally occur in a plasma due to its low resistivity. Since the typical current system in a plasma has a long L/R decay time, the plasma electric field from $E(t) = \eta(t)j$ varies rapidly with the level of the plasma turbulence. One of the well-documented settings of current-driven turbu-

lence is the ionosphere (Ref. 6, pp. 167–182 and 397–419). In this weakly ionized plasma, large currents are driven by the magnetospheric coupling to the solar wind dynamo. Both the Buneman (7) two-stream instability at high drift velocities and the $\boldsymbol{E} \times \boldsymbol{B}$ gradient instability at low drift velocities (8,9) are well-documented sources of plasma turbulence. Here we summarize the first considerations for determining the plasma turbulence and resistivity.

Two-Stream Instability

In the initial phase of a plasma carrying a high current, the electron drift velocity relative to the ions $u \equiv -j/en_e$ exceeds the electron thermal velocity $v_e = (k_B T_e/m_e)^{1/2}$. These conditions produce a strong, unstable electrostatic wave with an intermediate phase velocity that grows until it traps most of the electrons. The trapping mechanism thermalizes the electron distribution to the new, high temperature $T_e \simeq 4(m_i/m_e)^{1/3} m_e u^2$ which may be described as a turbulent heating with the effective collision frequency $\nu_{\text{eff}} \simeq 0.2\omega_{pe}(m_e/m_i)^{1/3}$ as shown in the laboratory by Hamberger and Jancarik (10). At the end of the turbulent heating of the electrons, the plasma current is still present, but now the plasma instabilities are kinetic with the ion acoustic wave turbulence driven by the positive slope on the drifting electron velocity distribution function.

Ion Acoustic Turbulence Driven by the Plasma Current

After the electron temperature rises to the level where the drift parameter $u/v_e < 1$ the uniform plasma has unstable ion acoustic waves that provide an anomalous resistivity η and thermal diffusivity χ. There is also a condition that $T_e/T_i \gg 1$ for the ion acoustic turbulence to be strong. When the large T_e/T_i condition is not satisfied, the nonuniformity or gradient drift velocity must be present for the system to be unstable. This is the usual regime of laboratory plasma confinement experiments and is the topic of the section entitled "Spatial-Gradient-Driven Turbulence in Magnetized Plasma."

When the ion acoustic turbulence is unstable, the system exhibits the effective collision frequency that rises linearly with u/v_e as shown in Fig. 1 for $u/v_e \lesssim \frac{1}{2}$. The higher u/v_e region is the transition to the Buneman two-stream turbulence. The turbulence exists as a cone-shaped spectrum of wave vectors pointing in the direction of the electron drift velocity $\boldsymbol{u}$ measured with respect to the ion rest frame. An ion acoustic spectrum is shown in Fig. 2. The waves receive energy and momentum from the electrons and deposit energy and momentum in the ions. The response of the ions depends on their mass and collision frequency with the neutrals. For collisionless, light (hydrogenic) ions, the turbulence produces a fast ion tail on the ion velocity distribution. Ion energies beyond $5T_e$ are produced and the density n_t of the ion tail varies roughly as $n_t/n_e \simeq (m_e/m_i)^{1/4}$. In plasmas with a mixture of ion species, the hydrogenic component is easily accelerated to form the energetic ion tail and thus shuts off the linear growth mechanism (11). Thus, the turbulence tends to appear in bursts. The transport coefficients are given in Horton et al. (12).

For complex structured signals $\phi(\mathbf{x}, t)$, typical of what is meant by the term *turbulence,* the standard measure of the coherence of the signals is the two-point, two-time correlation

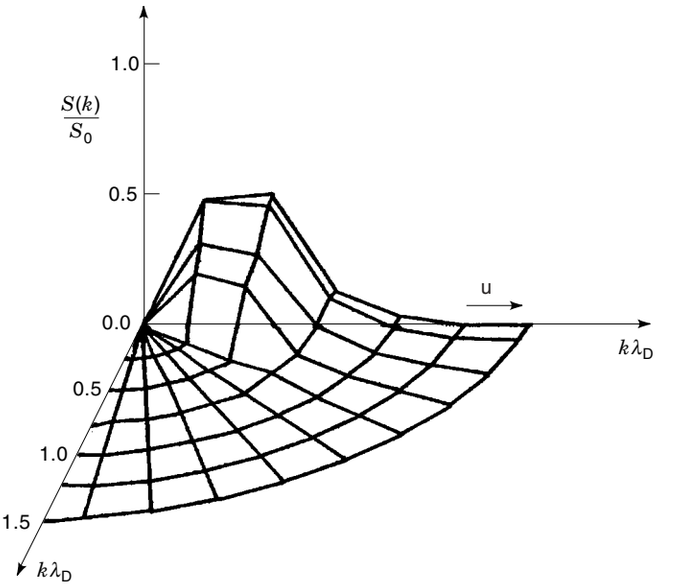

Figure 2. Spectral distribution of wave vectors for current driven turbulence in unmagnetized plasma. The $\boldsymbol{k}$ vectors form a cone in the direction of the electron drift velocity $\boldsymbol{u}$. The shape of the cone is determined by the balance of the linear growth rate and the nonlinear scattering of the waves (12).

function

$$C_{12}(\mathbf{x}, t_1, \mathbf{x}_2, t_2) = \langle \phi(\mathbf{x}_1, t_1)\phi(\mathbf{x}_2, t_2) \rangle \tag{1}$$

where the average $\langle\ \rangle$ is taken over a time period that contains many oscillations of the associated field. The correlation functions for the plasma electric potential ϕ and the fluctuations of the electron density $\delta n_e = n_e(\mathbf{x}, t) - \langle n_e \rangle$ are the principal structure functions of use in plasma turbulence research. The dependence of C_{12} on $\mathbf{r} = \mathbf{x}_2 - \mathbf{x}_1$ and $\tau = t_2 - t_1$ is strong, decaying to small values for large $\mathbf{r}$, τ; and the dependence on $\mathbf{R} = (\mathbf{r}_1 + \mathbf{r}_2)/2$ and $t = (t_1 + t_2)/2$ is weak for turbulent systems. In the physics idealization of homogeneous, stationary turbulence $C_{12} \to C_{12}(\mathbf{r}, \tau)$ independent of $\mathbf{R}$ and t. It is evident that $C_{12}(\mathbf{r}, \tau)$ is maximum at $\mathbf{r} = 0$, $\tau = 0$ where $C_{12} \to \langle \phi^2 \rangle$ and falls to low values for large $|\mathbf{r}|$ or $|\tau|$. These properties provide the definition of the correlation distances Δx_c, Δy_c, Δz_c and correlation time τ_c by choosing a critical point for the fall-off of $C_{12}/C_{12}(0)$ usually taken as the $1/e$-point of the envelope.

For the ion acoustic turbulence the correlation function of the electrostatic potential turbulence is shown in Fig. 3 from the experiment of Stenzel (12a). In Fig. 3(a) the decay of the two-point correlation function of separation Δz of the two-space points along the direction of the current $\mathbf{j} = -en\mathbf{u}$ driving the turbulence is shown for all other separations ($\Delta x = \Delta y = \tau = 0$) equal to zero. In Fig. 3(b) the constant level contours of C_{12} of the correlation function for separations in Δz along the current and in an orthogonal direction Δy are shown. Note that the central maximum (approaching 40 units) occurs at the $\Delta y = \Delta z = 0$ point and the correlation length ($\Delta y_c \cong 6$ mm) perpendicular to the current is longer than the correlation parallel to the current $\Delta z = 4$ mm. This anisotropy of the turbulence is a characteristic of plasmas due

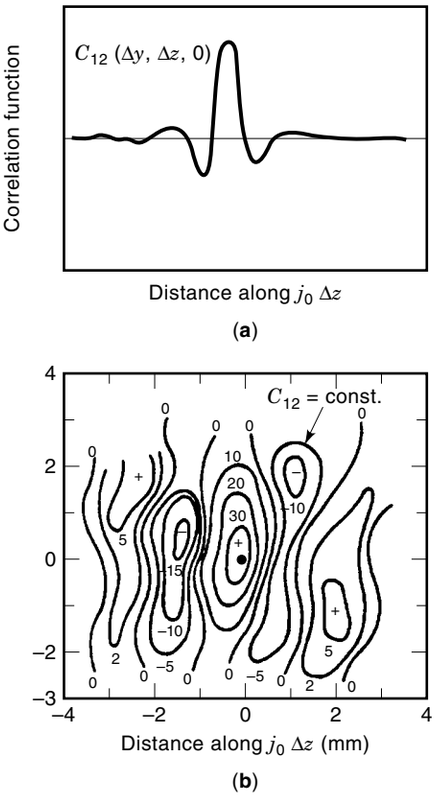

Figure 3. Characterization of the turbulent electrostatic potential by the two-point correlation function C_{12} in Eq. (1): (a) Decay of the correlation function with separation of the two points along an axial line parallel to the current; (b) Oscillatory decay of the correlations for two points in the y–z plane where the $\hat{y}$ direction is perpendicular to the current and $\hat{z}$ is the parallel direction (courtesy of Stenzel).

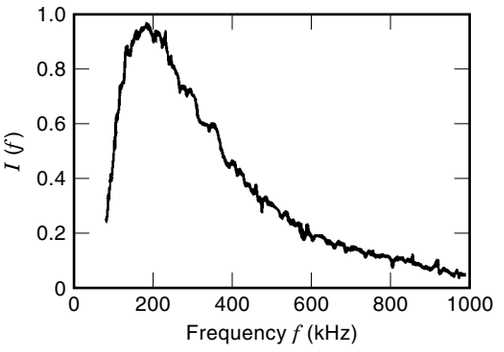

Figure 4. Frequency spectrum of ion acoustic turbulence showing the broadband potential fluctuation spectrum with short correlation time $\tau_c = 1/\Delta\omega \cong 0.5$ μs. The spectral distribution decreases slightly faster than $1/\omega$ between the low-frequency cut-off due to nonlinear effects and a high-frequency limit due to landau damping on the thermal ions (courtesy of Stenzel).

to the preferred directions of unstable wave propagation associated the geometry and the magnetic fields in the plasma systems.

For broadband turbulence there is a simple rule for estimating the correlation time τ_c and correlation lengths $\Delta\mathbf{r}_c$ from the spectral width of the power spectrum $I(\mathbf{k}\omega)$ defined by the Fourier transform of the correlation function $C_{12}(\mathbf{r}, \tau)$. The correlation time is given by $\tau_c = 1/\Delta\omega$ and the correlation length $\Delta z = 1/\Delta k_z$ where $\Delta\omega = \omega_{\max} - \omega_{\min}$, $\Delta k_z = k_{\max} - k_{\min}$ are the widths of the highest levels of the fluctuation power spectrum $I(\mathbf{k}, \omega)$. As an example, the ion acoustic turbulence in the Stenzel experiment is shown in Fig. 4 where a spectrum consistent with turbulence theory has been reported. The spectral width from the $1/e$ point is approximately 400 kHz, consistent with the directly measured $\tau_c = 3$ μs correlation time. Physically, the correlation time τ_c is the maximum time interval over which the field, in this case the electrostatic potential, maintains a given structure. In the next correlation time the complexion, or structure, of the field is qualitatively different.

SPATIAL-GRADIENT-DRIVEN TURBULENCE IN MAGNETIZED PLASMA

In nonuniform, magnetized plasmas the ion acoustic waves are modified into two branches with different parallel phases velocities due to the presence of the diamagnetic currents $\boldsymbol{j}_a = e_a n_a \boldsymbol{v}_{da}$ required from the $\boldsymbol{j}_a \times \boldsymbol{B} = \nabla p_a$ force balance. Here, each charged particle species is designated by the subscript a. In a sense, the relevant drift velocities for driving the plasma turbulence change to the small diamagnetic drift velocities $v_{da} = T_a/e_a B L_{pa} = (\rho_a/L_{pa})v_{Ta}$, where $L_{pa}^{-1} = -\partial_x \ln p_a(x)$. Even for small values of ρ_a/L_{pa}, these diamagnetic currents drive low-frequency ($\omega \ll e_a B/m_a$) waves with $\boldsymbol{k}$ almost parallel to $\boldsymbol{B} \times \nabla p_a$ unstable. These waves are called drift waves, and their effect is to produce a cross-field transport of particle energy and momentum. A direct spectroscopic measurement of the turbulent transport of injected impurity ions is given in Ref. 13.

Drift Waves in the Laboratory

The collisional drift waves with growth rates determined by resistivity η and thermal diffusivity χ_e were the first drift waves to be discovered and thoroughly investigated (14). The identification was made in low-temperature steady-state plasmas produced by thermal (contact) ionization of Alkali elements (principally cesium and potassium) in long cylindrical devices with closely spaced Helmholtz coils. Correlations between the observed potential-density waves with the properties predicted by the linear dispersion relation and the single-wave finite amplitude formulas (15) were used to establish that the radially localized, 10 kHz rotating wave structures were the drift waves. The dimensionless density $\tilde{n}/n$ and potential $e\tilde{\phi}/T_e$ waves are approximately equal amplitude sinusoidal oscillation with $\tilde{n}$ leading $\tilde{\phi}$ by 30° to 45° in phase. Figure 5 shows the drift wave potential and density isolines. Vortex dynamics has also been observed in the plasmas produced in these devices called Q-machines. Here Q stands for quiet. In the experiments of Pécseli et al. (16,17), externally excited vortices of like signs were shown to coalesce into one vortex. Vortices of opposite signs were reported to interact with each other forming a dipole vortex pair.

A variety of drift-type instabilities relevant to toroidal magnetic fusion devices, including the trapped electron modes by Prager et al. (18), the trapped ion instability by Slough et al. (19), and the collisionless curvature-driven trapped parti-

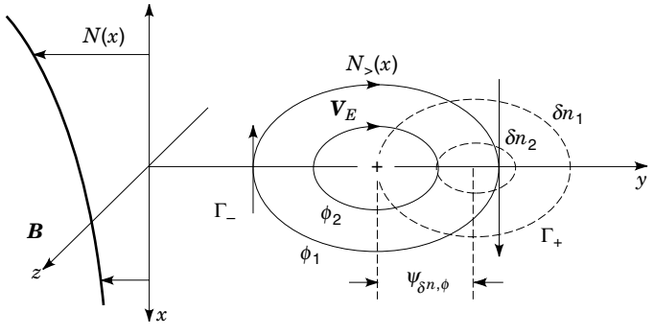

Figure 5. A segment of a drift wave fluctuation showing the variation of the electrostatic potential and the density perpendicular to the magnetic field at a given instant of time. The contours of ϕ in the plane perpendicular to $\boldsymbol{B} = \boldsymbol{B}_z$ are the stream lines of the $\boldsymbol{E} \times \boldsymbol{B}$ particle motion. The potential and the density variation are out of phase by $\psi_{\delta n,\phi}$, producing the net downward flux.

cle mode by Scarmozzino et al. (20) have been produced and identified in the Columbia linear machine (CLM).

The drift wave driven by the radial ion temperature gradient in a collisionless cylindrical plasma was demonstrated in the modified Columbia linear machine by Sen, Chen, and Mauel (21) by using biased wire screens to create a $T_{i\|}(r)$ gradient sufficient to excite an $m = 2$, 10 kHz (in the plasma frame) drift wave oscillation. The toroidal ITG mode driven by the magnetic curvature was also produced and identified by Chen and Sen (22) in the same machine. In the CLM experiments the plasma is in a steady state like the Q-machine experiments except that the plasma temperatures are an order of magnitude higher ($T_i \gtrsim T_e \sim 6$ eV) and the density is lower ($N \sim 10^9$ cm^{-3}), giving the collisionless condition ($\nu < \omega_k$) for waves with angular frequency ω_k in the working gas of hydrogen. There are approximately 15 ion gyroradii in the plasma radius.

Drift waves were found in the transient plasmas produced in the multipole confinement devices that were both linear and toroidal devices with strongly varying $\boldsymbol{B}$ fields from parallel conductors carrying large currents from external power supplies. The multipole plasmas of hydrogen, helium, and argon were produced by microwave frequency heating. The theory for the drift waves in the multipole takes into account the localization of the unstable oscillations to regions of unfavorable gradient B and curvature particle drifts and the shear in the helical $\boldsymbol{B}(\boldsymbol{x})$ field (22a). These experiments provided further evidence for the universal appearance of drift waves in confinement geometries. The correlation of drift wave theory with the multipole and spherator experiments are described in Section 3.3 of the Horton (3) review article. The main result to be noted here is that the experiments show that increasing the magnetic shear reduces the fluctuation amplitudes (23). The multipole devices are unique in being able to continuously vary the magnetic shear parameter strength from zero to of order unity. Even with the strongest magnetic shear, however, the fluctuations were not eliminated.

The magnetic shear plays a central role in the linear and nonlinear theory of the cross-field transport consistent with the role of shear on the fluctuations measured in these experiments. In recent theory and experiments for tokamak confinement devices the combined roles of $\boldsymbol{E}_r \times \boldsymbol{B}$ sheared flows and magnetic shear are known to produce enhanced confinement regimes (24,25). The improved confinement occurs over narrow radial regions giving rise to new confinement regimes with internal transport barriers (26–28). Table 1 gives the high-performance fusion plasma parameters achieved with internal transport barrier in the JT60U machine (26). The principal tools available for understanding these changes in transport are the dependence of drift wave turbulence on the system parameters, especially the magnetic shear in $\boldsymbol{B}(\boldsymbol{x})$ and mass flow shear in the hydrodynamic flow velocity $\boldsymbol{u}(\boldsymbol{x})$.

In tokamaks the identification of drift waves in the core plasma came from the microwave scattering experiments (29) and infrared CO_2 laser scattering experiments (30,31). These measured fluctuations were explained in the context of drift waves existing at the mixing-length level of saturation, taking into account the response of the trapped electrons in the drift-wave dissipation. Subsequently, many experiments around the world have observed the universal appearance of a broad band of drift wave fluctuations with $\omega/2\pi \simeq 50$ kHz to 500 kHz at $k_\perp = 1$ cm^{-1} to 15 cm^{-1} in toroidal confinement devices for both the tokamak and helical-stellarator systems. Many fluctuation and transport studies in toroidal confinement facilities around the world, including TFTR, Alcator, TEXT, TORE SUPRA ATF, Heliotron, JFT2M, and ASDEX, were undertaken in the 1980s and 1990s that have confirmed these initial findings of drift wave turbulence and the associated radial turbulent transport.

A basic physics research program on plasma fluctuations and anomalous transport was carried out from 1982 to 1994 in the TEXT tokamak at The University of Texas at Austin. This experiment provided the most complete correlated data sets of core fluctuations from five $k_\perp$ values (2, 4.5, 7, 9, 12 cm^{-1}) from far-infrared (FIR) laser scattering, complex probe arrays for edge turbulence, the heavy ion beam probe (HIBP) for measurements of the radial electric field E_r, and the space–time localized fluctuating potential $\tilde{\phi}$ in addition to the usual complement of spectrometers, interferometers, bolometers, and magnetic coils for determining the state of the plasma. A review of the FIR and HIBP data, as well as other diagnostics, leading to the conclusion that the drift waves are present and responsible for the transport, is given in Bravenec et al. (32).

A review of the diagnostics on TEXT and other tokamaks is given by Gentle (33). Table 2 gives the plasma parameters and the drift wave turbulence characteristics for TEXT and the approximately twice larger TFTR tokamaks. There is substantial supporting evidence in the high-level edge fluctuations data for resistive-interchange turbulence giving χ_{rg}.

Table 1. JT-60U High-β_p Experiment 17110 with Internal Transport Barrier: Phase I

R/a	3.1 m/0.7 m
B_ϕ	4.4 T
I_p	2 MA
P_{NBI}	27 MW
$n_D(0)$	4.1×10^{19} m^{-3}
$T_i(0)/T_e(0)$	38 keV/12 keV
$n_D \tau_E T_i$	1.1×10^{21} m$^{-3} \cdot$ s $\cdot$ keV
$v_\phi(0)$	-100 km/s

Table 2. Plasma Drift Wave Parameters

Parameter	TFTR	TEXT
Magnetic field	4.8 T	2 T
Major/minor radii	2.45 m/0.8 m	1.0 m/0.27 m
Electron temperature	6 keV	500 eV
Density n_e and	4×10^{13} cm^{-3}	3×10^{13} cm^{-3}
Gradient length L_n	20 cm	10 cm
Drift velocity v_d	3×10^5 cm/s	1×10^5 cm/s
k scattering experiment	1–20 cm^{-1}	1.5–15 cm^{-1}
ω scattering experiment	10–500 kHz	10–1000 kHz
$\tilde{n}_e/n_e$	5×10^{-3} to 0.02	0.01–0.1

Other drift turbulence is observed due to parallel shear flow, impurity drift modes, and recombination ionization. In the core plasma the dissipative trapped electron mode dominates in TEXT (32). In contrast to the ohmic heated TEXT experiments, for auxiliary heated plasmas where the Ohmic heating is a fraction of the total input power, the ion-temperature-gradient-driven drift wave is the dominant driving mechanism for the drift wave turbulence. The TEXT experiments were ohmic discharges with toroidal magnetic fields $B = 2$ T, plasma current $I = 200$ kA to 400 kA, and inductive loop voltage $\mathscr{E}_l = 2V$ from the iron core transformer. The discharges produced hydrogen plasmas with $T_e \lesssim 2$ keV and $T_i \lesssim 1$ keV from the collisional resistivity. In contrast, the major fusion confinement experiments have high-power neutral beam injection (NBI) systems providing injected powers $P_b = 5$ MW to 30 MW producing $T_e \leq 8$ keV and $T_i \leq 40$ keV. Thus, the nature of the instability driving the plasma turbulence switches from the electron temperature gradient $T_e'(r)$ parameterized by

$$\eta_e = \frac{\partial_r \ln T_e}{\partial_r \ln n_e} \tag{2}$$

to the ion temperature gradient $T_i'(r)$ parameterized by

$$\eta_i = \frac{\partial_r \ln T_i}{\partial_r \ln n_i} \tag{3}$$

in going from ohmic discharges in TEXT and ALCATOR to the high-power NBI heated discharges in TFTR, JET, DIII-D, and JT60U. The energy-momentum deposition profiles and magnitudes from the auxiliary heating become key control parameters in the later experiments. The latest results for the two major fusion laboratories with billion-dollar tokamaks are found at www.jet.uk and www.jt60.naka.jaeri.go.ip. Currently, the JET machine has the record of 13 MW of peak fusion power with a ratio of fusion power to net input power Q of 60%.

The conclusion of the TEXT experiment is that the drift wave fluctuations account for both the particle and thermal energy transport to the edge of the large Ohmic heated tokamak. At the extreme edge the plasma is in contact with a metallic diaphram where collisional and radiative losses dominate the transport and cooling of the plasma. The same conclusion that the small-scale drift wave turbulence determines the radial transport properties of the plasmas appears to apply to the largest ($I \gtrsim 2$ MA) tokamaks. There is some indication that the very core of the large machines may enter a quieter regime with lower transport levels (33a).

Physics of Plasma Transport and the Propagation of Disturbances

Now we analyze the ion motion in the $\boldsymbol{E} \times \boldsymbol{B}$ convection. For the small, localized excess of ion charge shown in Fig. 5 the

$$\boldsymbol{v}_E = \frac{c\boldsymbol{E} \times \boldsymbol{B}}{B^2} \tag{4}$$

convection rotates plasma clockwise around the potential maximum $\phi > 0$, which is also the density and electron pressure maximum in the adiabatic response. Now, if the ambient plasma is uniform ($\partial_x n_a = \partial_x T_i = 0$) across the convection zone, then the cell rotates without plasma transport. When the plasma has an x-gradient of density (pressure), however, there is a rapid transport of the structure along the symmetry direction $\hat{\boldsymbol{y}}$ with a small diffusive transport across an $x =$ const surface. The speed of the localized structure in Fig. 5 along the symmetry direction is approximately the electron diamagnetic drift speed $v_{de} \equiv cT_e/eBL_n$, where $L_n^{-1} = -\partial_r \ln N$. The analytical description of the net convective flux particle and thermal fluxes across a given surface S is given by

$$\Gamma_a = \frac{1}{S}\int_S n_a \boldsymbol{v}_E \cdot d\boldsymbol{a} = -D_{11}\frac{dn_e}{dx} - D_{12}\frac{dT_e}{dx} \tag{5}$$

$$q_a = \frac{3}{2S}\int_S n_a T_a \boldsymbol{v}_E \cdot d\boldsymbol{a} = -D_{21}\frac{dn_e}{dx} - n_e D_{22}\frac{dT_e}{dx} \tag{6}$$

In the absence of the phase shift $\delta n - \phi$ in Fig. 5, the transport vanishes. In the proper set of flux-driving gradient variables the transport matrix has Onsager symmetry (34). The Onsager symmetries guarantee the correct thermodynamic properties for the system.

For the positive potential structure in Fig. 5, the clockwise $\boldsymbol{E} \times \boldsymbol{B}$ rotation brings higher density $N_>$ (and higher pressure $N_> T_e$) plasma to the right and lower density $N_<$ (pressure) to the left, resulting in a shift of the maximum density and potential, linked through the electron response by $\delta n_e \cong n_e(e\phi/T_e)$, to the right. The speed of the translation is proportional to the gradient of the density $L_n^{-1} = -\partial_r \ln N$ and inversely proportional to the strength of the magnetic field B. The speed also increases with electron temperature T_e since the potential fluctuation $e\phi$ scales up with T_e. For a negative potential structure the $\boldsymbol{E} \times \boldsymbol{B}$ rotation is counterclockwise, but the structure moves to the right with same speed (in the limit of small $e\phi/T_e$) since now lower-density plasma is brought to the right, shifting the minimum in that direction. Now, the ion density at this location builds up in the time δt equal to that of the original electron maximum $\delta n_e = N(e\phi/T_e)$ when the condition

$$\delta n_i = -\frac{\delta t c\phi}{B\delta y}\frac{\partial N}{\partial x} = N\frac{e\phi}{T_e} \tag{7}$$

is satisfied. In the last step we use quasineutrality taking $\delta n_i = \delta n_e = N(e\phi/T_e)$, which is valid for fluctuations that are large compared to the Debye length. During the time δt the convection moves the maximum of the structure to the right by $\delta y = v_{de}\delta t$, where

$$v_{de} = \frac{\delta y}{\delta t} = -\frac{cT_e}{eBN}\frac{\partial N}{\partial x} \tag{8}$$

The x-displacement of the plasma during this motion is $\xi_x = v_x \delta t = -\delta t \delta\phi / B \delta y$. When this displacement becomes comparable to δx the motion is nonlinear, leading to the formation of nonlinear vortex structures. Locally, the plasma is mixed over the length δx in one rotation period when the amplitude $\xi_x = \int^t dt' v_{Ex} = \delta x$. The nonlinear problem is treated in *Chaos and Structures in Nonlinear Plasmas* by Horton and Ichikawa (35).

Drift Wave Diffusivities and the Ion Inertial Scale Length

It is conventional in the study of drift waves and transport to introduce gradient scale lengths and reference diffusivities. Thus, the length L_n is defined as the density gradient scale length through the relation $1/L_n = -\partial_x \ln N$. The temperature gradient scale length L_T is defined similarly. The space–time scales of the waves lead to two different dimensional scalings for the plasma diffusivities. The reference diffusivities are the Bohm diffusivity

$$D_B = \frac{T_e}{eB} \tag{9}$$

and the drift wave diffusivity

$$D_{dw} = \left(\frac{\rho_s}{L_n}\right)\left(\frac{T_e}{eB}\right) \tag{10}$$

also commonly called the gyro–Bohm diffusivity in reference to the factor $\rho_s/L_n \ll 1$. Here $\rho_s = (m_i T_e)^{1/2}/eB$ is effective gyroradius parameters for hot electrons $T_e \gtrsim T_e$. Clearly, the scaling of the Bohm and gyro–Bohm diffusivities are markedly different with $D_B \propto T_e/B$ independent of the system size while $D_{dw} = T_e^{3/2}/B^2 L$, decreasing with the system size. There is a long history of confinement scaling studies that have correlated the thermal and/or particle confinement with either the Bohm or the drift wave scaling laws. The issue is still actively debated as to which transport scaling is to occur under given confinement conditions (36). In short, the Bohm [Eq. (9)] scaling arises from *mesoscale* drift wave structures $\Delta x = (\rho_s L_T)^{1/2}$ and thus is expected near marginal stability (37–40). When the convective cells size reduces to $\Delta x = \rho_s$ the drift wave diffusivity [Eq. (10)], more commonly called gyro-Bohm, applies.

A compendium of thermal diffusivity formulas collected from the literature on drift wave turbulent transport is given by Connor and Wilson (41). Equations (9) and (10) must be multiplied by dimensionless functions of the system parameters to explain transport in a particular device. Currently, large-scale particle simulations are used to address this issue from first principle calculations (42,43).

In defining the dimensionless gyroradius parameter ρ_*, it is usual to replace the space–time varying length L_n with the relatively constant value a of the plasma minor radius. Thus, a key issue is the scaling of plasma confinement systems with

$$\rho_* \equiv \frac{\rho_s}{a} \tag{11}$$

(44,45). Drift wave theory is able to account for confinement scaling either as D_B or $\rho_* D_B$. Transport dependent on ρ_* depends on the average mass m_i of the working gas ions since $\rho_* = (m_i T_e)^{1/2}/eB$.

The Perkins et al. (45), Petty et al. (36), and Erba et al. (2) studies present evidence for the Bohm-like scaling of transport. Power balance in the JET discharge up to 7 MA of plasma current is obtained with $\chi_e = \alpha_e q^2 (a/L_p) D_B$ and $\chi_i = \alpha_i \chi_e + \chi_i^{\text{neo}}$ with $\alpha_e = 2.1 \times 10^{-4}$ and $\alpha_i = 3.0$ (1,2). Here $1/q(r) = RB_\theta / rB_T$ gives the local pitch of the helical magnetic side line.

The fluctuation measurement at wavenumbers $k_\perp \lesssim 1$ cm^{-1} require the techniques of reflectometry (46,47) and the indirect method of beam emission spectroscopy as in the Durst et al. (48) experiment.

Let us close by showing the evidence from the FIR scattering experiment in the core of the TEXT experiment (49,50). Figure 6 shows the peak of the frequency of the electron density fluctuations inferred from the dynamical scattering factor $S(k_\perp, \omega)$ versus the wavenumber $k_\perp$ from the scattering geometry. The frequency of the spectrum in the lab frame follows $\omega = \omega_k(\eta_i) + k_\theta v_E$ to a good approximation where $v_E = -cE_r/B$ is the Lagrangian velocity of the plasma (ions and electrons) relative to the laboratory frame of reference and $\omega_k(\eta_i)$ is the drift wave frequency in the plasma frame. The plasma rest frame frequency ω_k is shown by dotted lines for the range of $\eta_i = \partial \ln T_i / \partial \ln n_i$ values in this experiment. The corresponding laboratory frame frequencies are given by the dashed lines. To find the transformation velocity v_E, and thus the Doppler shift, the HIBP diagnostic is used to determine the radial electric field $E_r(r)$. Quasilinear theory (QT) predicts the spectrum of density fluctuations

$$S(\boldsymbol{k}, \omega) = \frac{S_0}{VT}\left\langle \left| \frac{\delta n_e(\boldsymbol{k}, \omega)}{n_e} \right|^2 \right\rangle \simeq I(\boldsymbol{k}) \delta(\omega - \boldsymbol{k} \cdot \boldsymbol{u} - \omega_{\boldsymbol{k}})$$

where V and T are the sample volume and time interval. Renormalized turbulence theory (RNT) gives a Lorentzian spec-

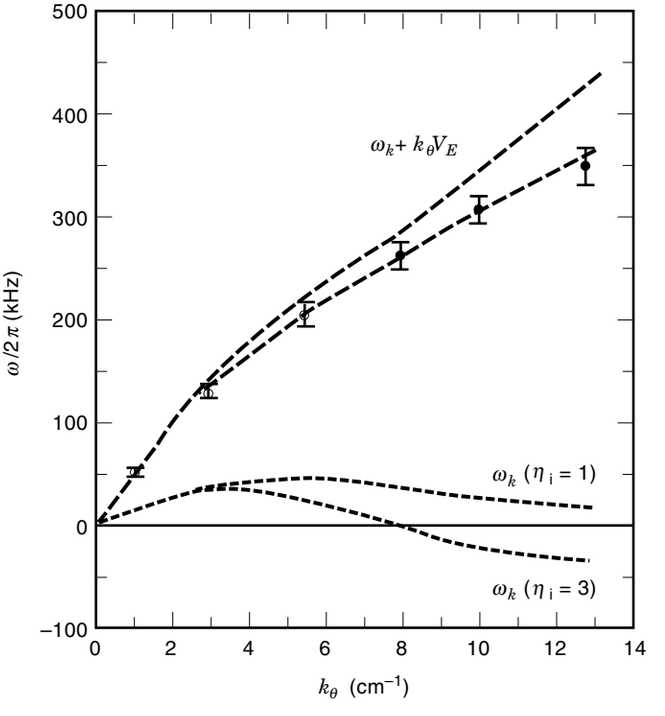

Figure 6. The measured frequency spectrum obtained from far-infrared laser scattering from the electron density fluctuations from the drift waves in the TEXT Tokamak. (Courtesy of Brower).

tral distribution

$$S^{\rm rn}(\boldsymbol{k},\omega)=\frac{I(\boldsymbol{k})\nu_{\boldsymbol{k}}}{(\omega-\omega_{\boldsymbol{k}})^2+\nu_{\boldsymbol{k}}^2} \tag{12}$$

with the turbulent decorrelation rate

$$\nu_{\boldsymbol{k}}\simeq\langle(\boldsymbol{k}\cdot\boldsymbol{v}_E)^2\rangle^{1/2}\simeq\frac{ck_\perp^2\tilde{\phi}}{B} \tag{13}$$

The agreement of the peak of the FIR measurement of $S(k, \omega)$ in Fig. 6 and the theoretical formulas for the drift waves is the direct signature of the drift wave turbulence.

The main features of the measured fluctuations are explained by drift waves and the drift wave turbulence. Comparing the fractional fluctuation level $\tilde{n}/n$ from the early smaller machines ATC (29) with the intermediate size TEXT and the large TFTR machine shows that the core fractional fluctuation level scaling is consistent with $(\rho_s/a)^\alpha$ with an exponent between $\frac{1}{2}$ and unity.

In a review article it is important to point out parallels with other areas of physics. The closest and most important parallel to plasma drift waves is the analogy with the Rossby waves and vortices in geophysical atmospheric and oceanographic disturbances with periods long compared to the rotational period of the planet. Hasegawa and Mima (51,52) and Hasegawa et al. (53) develop the limit in which the two models become isomorphic. The correspondence is due to the Coriolis force having the same mathematical form as the Lorentz force. The analogy was also recognized by Petviashvili (54) which led to the first rotating parabolic water tank experiments by Antipov et al. (55,56) in Kurchatov and by Antonova et al. (57) in Tiblisi. This aspect of the drift-wave–Rossby problem is found in the Horton and Hasegawa (58) article in the special issue of CHAOS devoted to such geophysical vortex structures. Further development of the theory from the plasma physics perspective is given in *Chaos and Structures in Nonlinear Plasmas* by Horton and Ichikawa (35).

Scaling Laws of the Ion Temperature Gradient Turbulent Transport

The most important instability with respect to the limits on the ion thermal confinement for nuclear fusion is the ion temperature gradient (ITG) instability. This drift wave instability goes by both the name ITG and the eta-i ($\eta_i\equiv L_n/L_{T_i}$) mode due to the key dimensionless parameter η_i that measures the strength of the ion temperature gradient. For a specific toroidal machine with major radius R, it is advantageous to use the gradient parameter $\mu_i=R/L_{T_i}$ since, unlike L_n, the major radius R of the machine is fixed. In certain regimes there is a well-defined critical value $\eta_{i,\rm crit}$, starting at the minimum of $\frac{2}{3}$, above which there is a strong drift wave instability producing anomalous ion thermal flux q_i.

First studies of the ITG turbulent transport were naturally concerned with regimes where the mode growth per wave period $\gamma_{\boldsymbol{k}}^{\max}/\omega_{\boldsymbol{k}}$ is substantial (≥ 0.1). The $\gamma_{\boldsymbol{k}}^{\max}$ occurs approximately at the wavenumbers $k_y\rho_i\simeq(1+\eta_i)^{-1/2}\ll 1$. In this regime the mixing scale length for an isotropic fluctuation spectrum ($\lambda_x\simeq\lambda_y$) of wavelengths λ gives $\chi_i\sim\lambda_\perp^2\gamma_{\max}\simeq(\rho_i/L_{T_i})(cT_e/eB)\,g(\eta_i, s, q, \epsilon_n)$ at the fluctuation levels $\tilde{n}/n=e\tilde{\phi}/T_e\simeq\rho_s/L_{T_i}$ as known from theory and associated with the experiment in Fig. 4. Parameters for such a regime are $\eta_i=3$, $S=L_n/L_s=0.1$, and $\tau=T_e/T_i=1$ as in the three-dimensional (3-D) FLR fluid simulation (4,58a) and the gyrofluid simulation (58b,59,59a).

The 3-D-slab model simulations (4,58a) show that the ion thermal diffusivity is

$$\chi_i^{\rm slab}=0.3\left(\frac{L_s}{L_n}\right)^{1/2}\frac{\rho_s}{L_n}\frac{cT_e}{eB}(\eta_i-\eta_c) \tag{14}$$

for the magnetic–shear parameter $S=L_n/L_s>S_1=0.05$ and $\eta_c\leq\eta_i\lesssim 4$. For small shear $S<S_1$ the scaling $S^{-1/2}$ is too strong and the parameterization with S is given as exp $(-S/S_0)$ in (58a) and as $q/(S+S_0)$ in Kotschereuther et al. (58c) and Waltz et al. (59,59a). When the turbulence level is high we expect S_0 independent of ρ_*: For low turbulence levels, S_0 is proportional to ρ_*. Near the critical gradient the exponent on $\eta_i-\eta_c$ in Eq. (14) becomes unity. The supporting nonlinear bifurcation analysis is found in Hamaguchi and Horton (58a).

For the regime of $\eta_i\gg 1$ the density gradient parameter L_n drops out of the system and the parameterization of the 3-D simulations gives $\chi_i=0.8\,(\rho_s/L_T)(cT_i/eB)\,g(q, s, T_i/T_e)$. This is called the flat density regime where $\eta_i\gtrsim 3$ to 4.

In full toroidal models there are additional parameters. The instability in the toroidal system changes character from that in the cylindrical system. It is the linear eigenmode problem (59b) that determines how the plasma adjusts through the self-consistent field dynamics to the gradient driving mechanisms and the sheared toroidal magnetic field to obtain the fastest release of stored thermal energy contained in the pressure gradient.

In the toroidal regime the ion thermal diffusivity formula is the formula given by (59c):

$$\chi_i^{\rm HCT}=c_T\frac{q\rho_s}{sL_n}\frac{cT_e}{eB}[2\epsilon_n(\eta_i-\eta_c)]^{1/2} \tag{15}$$

with c_1 of order unity. Owing to the factor of q the confinement is inversely proportional to the product of self-field $B_p\approx I_p/a$ and the external toroidal field $B\cong B_\phi$. The peak of the growth rate driving the turbulence is at $k_y=\rho_s^{-1}[1/(1+\eta_i)]^{1/2}$. Near this wavenumber the phase velocity ω_k/k_y is changing from the electron diamagnetic direction for smaller $k_y\rho_s$ to the ion diamagnetic direction at larger $k_y\rho_s$. Thus, there is a critical wavenumber where the phase of the wave is stationary in the plasma rest frame and the mode grows exponentially at the interchange growth time $\tau=(RL_{T_i})^{1/2}/c_s$, which is on the order of a few microseconds.

In the absence of the ITG fluctuations ($\eta_i<\eta_c$) the calculation of the ion thermal flux in the torus is still a complicated problem due to the geometry and complex ion orbits. The collisional thermal flux for low collisionality $\nu_{*i}\equiv(\nu_i qR/v_{T_i})(R/r)^{3/2}\leq 1$ is from the random walk of the banana orbits formed by the guiding center drifts of the trapped ions. Most large tokamaks ($I>1$ MA) are in this low collisionality regime. The collisional thermal flux $q_i=-n_i\chi_i^{\rm neo}\,dT_i/dr$ (which is only one diagonal element of a large transport matrix) is given by Chang and Hinton (60) and Hirshman and Sigmar (60a). In the small $\epsilon=r/R$ limit the ion thermal diffusivity

from collisions is

$$\chi_i^{\text{neo}} = \nu_i \rho_{i\theta}^2 (0.66 + 1.88(r/R)^{1/2})(r/R)^{1/2} \tag{16}$$

where the 0.66 arises from the pitch angle scattering and the 1.88 arises from energy scattering (60b). Here $\rho_{i\theta} = q\rho_i/\epsilon$ and the post-factor of $(r/R)^{1/2}$ takes into account that only the trapped and barely passing ions, whose fractional density increases as $(r/R)^{1/2}$, contribute to the χ_i^{neo} in the banana regime. At larger collisionality $(R/r)^{3/2} > \nu_{*i} > 1$ the ion detrapping collision occurs before the banana orbit is formed. The ion thermal diffusivity from collisions in this regime is $\chi_i^{\text{neo}} = 2.6(v_i/qR)(q\rho_i)^2$.

The theoretical structure of the full transport problem treating the collective drift wave fluctuations and the collisional interactions on equal footing is given in a series of works by Sugama and Horton (60c,d) for electrostatic turbulence and by Sugama et al. (34) for electromagnetic turbulence. Both transport processes arise from the Coulomb interactions of the charged particles. The collision operator takes into account the thermal fluctuation levels at Debye length space scales $k\lambda_{\text{De}} \gtrsim 1$, while the drift wave takes into account the collective Coulomb interactions on space scales covering many Debye lengths $k\lambda_{\text{De}} \ll 1$.

The general procedure of predicting the $T_i(r)$ profiles from the energy–momentum deposition profiles for the evolution of the core plasma is carried out with transport codes. An example is shown in Fig. 7 from the IFS/JAERI collaborative analysis of an important discharge (60e). The normalized gradient scale lengths computed for the JT60-U discharge 17110 is shown in Fig. 7. The principal system and plasma parameters for the discharges are given in Table 1.

Recent deuterium discharges in JT60-U have reached sufficient plasma confinement in the presence of the drift wave turbulence to achieve conditions showing that the equivalent deuterium–tritium (D–T) plasma would have achieved fusion power breakeven. The D–T fuel is roughly 200 times more reactive than the deuterium–deuterium (D–D) fusion fuels at these ion temperatures. Extrapolations of the JET and JT60U parameters to a 20 MA tokamak predict a fusion power sufficient for ignition.

Resistive Drift Wave and Interchange Turbulence

The collisional drift wave is a paradigm for anomalous transport that has been extensively investigated with many different modelings. A particularly simple two-dimensional (2D) model, called the Hasegawa–Wakatani (61) model with an adiabaticity parameter α, has been investigated by Wakatani and Hasegawa (5), Krommes and Hu (61a), and Hu et al. (61b). To understand the origin of the simple α-model and to appreciate its limits, we briefly present the 3D resistive drift model.

For finite resistivity $\eta = m_e\nu_e/n_e e^2$ the parallel current carried by the electrons in Eq. (11) yields $j_\parallel = -(n_e e^2/m_e\nu_e)\nabla_\parallel(\phi - T_e/e \ln n)$ using the isothermal approximation $\delta p_e = T_e \delta n_e$. The collisional drift wave equation follows from the divergence of the current $\nabla \cdot \boldsymbol{j} = 0$ with the polarization current balancing $j_\parallel$ through $\nabla \cdot \boldsymbol{j}_p = -\nabla_\parallel j_\parallel = \eta^{-1}\nabla_\parallel^2(\phi - (T_e/e) \ln n)$ and the electron continuity equation. The rotational part of the plasma momentum for the vorticity $\nabla^2\varphi$ is equivalent to the current closure equation. The vorticity equation and the electron continuity equation give, in dimensional form,

$$\frac{m_i n c}{B_0}\frac{d}{dt}\nabla^2\varphi = \frac{B_0}{c}\nabla_\parallel j_\parallel + \hat{\boldsymbol{z}} \cdot \nabla p_e \times \nabla\Omega \tag{17}$$

$$\frac{d}{dt}(n_0 + n_1) = \frac{1}{e}\nabla_\parallel j_\parallel + \frac{cT_e n_0}{eB_0}\hat{\boldsymbol{z}} \cdot \nabla\left(\frac{n_1}{n_0} - \frac{e\varphi}{T_e}\right) \times \nabla\Omega \tag{18}$$

where $\nabla\Omega$ is the effective $\mathbf{g}$ force used to relate the curvature and gradient-B effects to the classical Rayleigh–Taylor instability. The computation of $\Omega(r)$ for the average curvature of the magnetic field line is extensively used in stellarator/heliotron research (62). The derivatives on the left side of Eqs. (17) and (18) are the $\boldsymbol{E} \times \boldsymbol{B}$ convective derivatives defined by $df/dt = \partial_t f + \boldsymbol{v}_E \cdot \nabla f$. The model equations (17) and (18) have a conserved potential vorticity ζ given by

$$\zeta = \frac{m_i c^2}{eB^2}\nabla_\perp^2\varphi - \ln n_0 - \frac{n_1}{n_0} - \Omega \tag{19}$$

The potential vorticity includes the influences of the density variations and the nonuniformity of the magnetic field. From the conservation of the potential vorticity $ds/dt = 0$ many of the complex vortical structures of the flow can be understood.

This 3-D model in Eqs. (17) and (18) has resistive drift waves driven by the density gradient $(\partial_x n_0)^2$ through the charge separation from finite $k_\perp^2\rho_s^2$ and has resistive interchange-driven modes from $\omega_*\omega_D > 0$, where $\omega_D = (ck_\theta T/eB)(d\Omega/dr)$ is the averaged grad-B/curvature drift frequency. The linear eigenmodes are of two types: localized to the rational surfaces where $k_\parallel = 0$ and global modes.

Wakatani et al. (63) carried out 3-D simulations of this system, and the results for one case are shown in Fig. 8. The density fluctuations are large and give a qualitative explanation of the similar tokamak and stellarator/helical device edge density fluctuations.

The electric potential, shown in the left column in Fig. 6, has the important property of developing an $m = 0/n = 0$ component with a well-defined circular null surface. This $\varphi_{0,0}(r, t) = 0$ surface partially blocks the turbulent losses from the core of the cylindrical model. For stellarators the $m = 1$, $n = 1$ rational surface is near the edge of the plasma and the dominant modes in this simulation are the $m = 3/n = 2$ and $m = 2/n = 1$ fluctuations and the $m = 0/n = 0$ background profile for $v_\theta = -cE_r/B$. These simulations with $\nu_e/\omega_{ce} = 1.4 \times 10^{-4}$ are too collisional to apply to the edge of tokamaks with $I > 1$ MA confinement devices (where $\nu_e/\omega_{ce} \lesssim 10^{-6}$).

Wakatani et al. (63) investigations of the model include an externally imposed electric field $E_r(r)$ exceeding the strength of self-consistently field generated from the $m = 0/n = 0$ modes. The $E_r < 0$ field suppresses the turbulence during the growth phases, but produces only a weak reduction of the flux in the saturated state. The collisionality dependence of the particle flux is shown to increase with ν_e for $\nu/\omega_{ce} < 10^{-3}$ and then to increase as $\nu_e^{1/3}$ for $\nu/\omega_{ce} > 10^{-3}$.

In the widely investigated reduced 2-D model of the Hasegawa–Wakatani equations the operator $\nabla_\parallel \to i\bar{k}_\parallel$ or $-i/\mathscr{L}_c$, where $\bar{k}_\parallel$ is the relevant mean parallel wavenumber and $\mathscr{L}_c$ is the connection length to the divertor end plates in the scrape-off layer (open field lines) modeling the new parameter α appears.

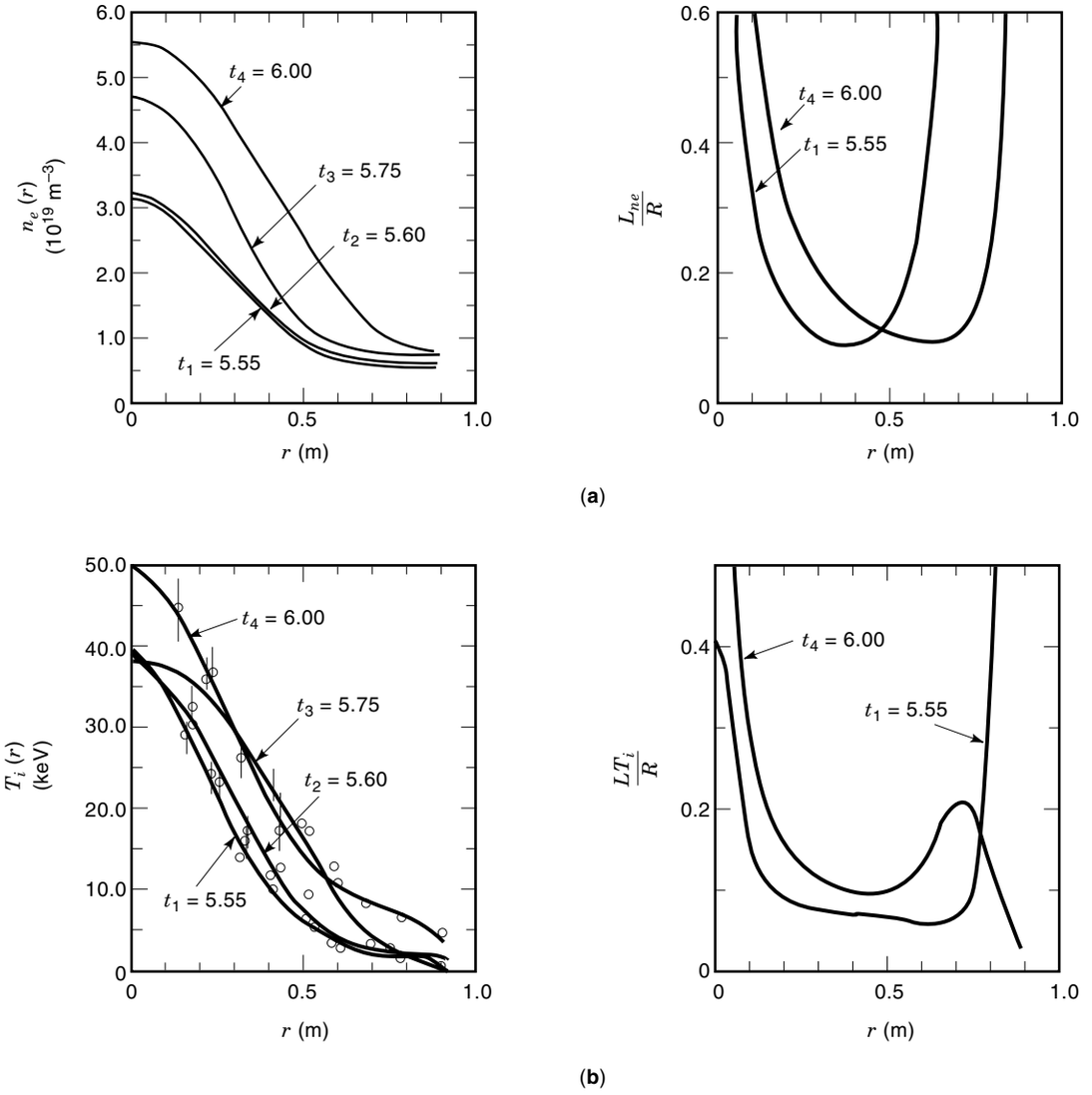

Figure 7. Evolution of the temperature and density profiles for the JT-60U experiment during the formation of the internal transport barrier at $r/a = 0.7$. (a) Smoothed density profiles used to compute the gradient scale lengths at four times during the growth of the core pressure from the internal transport barrier. The inset gives $\epsilon = L_{n_e}/R$. (b) Ion temperature profiles and the inset shows $\epsilon = L_{T_i}/R$.

The space–time units are changed to the local scales of ρ_s and L_n/c_s in these 2-D studies. The standard form of the Hasegawa–Wakatani 2-D model is then

$$\frac{d}{dt}(\nabla^2\phi) = \alpha(\phi - n) + \mu\nabla^4\phi \tag{20}$$

$$\frac{dn}{dt} = -\kappa\frac{\partial\phi}{\partial y} + \alpha(\phi - n) + D\nabla^2 n \tag{21}$$

where the viscosity μ and D are taken small, but finite to absorb all fluctuation energy reaching the smallest resolved space scales in the simulation system. The system's strong turbulence features a small α where $\alpha/\overline{\omega} \sim 1$, where $\overline{k}$, $\overline{\omega}$, $\overline{\gamma}$ are taken at the peak of the energy spectrum. Here the overbars on k, ω, γ denote a mean value near the peak of the energy spectrum E_k. One can show that $\overline{k} \approx \alpha^{1/3}$, $\overline{\gamma} \approx \alpha^{1/3}$, and $E\overline{k} \simeq \overline{\gamma}^2/\overline{k}^3 \simeq 1/\alpha^{1/3}$ (61a). In the large α limit the density $n \to \phi(1 + \mathcal{O}(1/\alpha))$ approaches the adiabatic limit and a weaker turbulence appears with $E_k \simeq \overline{\gamma\omega}/\overline{k}^3 \approx 1/\alpha$ since $\overline{\gamma} \sim 1/\alpha$, and $\overline{k} = \alpha^0$ and $\overline{\omega} = \alpha^0$ independent of α. These α-scalings in the small-α and large-α regimes have been verified by direct numerical simulation and the statistical closure method. The analytical closure method used here is a realizable Markovian closure (RMC). Figure 9 shows the good agreement between the direct numerical simulation (DNS) and the RMC closure calculation.

The new parameter $\alpha = k_\parallel^2 T_e/m_e\nu_e\omega_0$ measures the parallel electron diffusion in a characteristic wave period $(1/\omega_0)$ and determines the properties of the waves. For $\alpha \gg 1$ the elec-

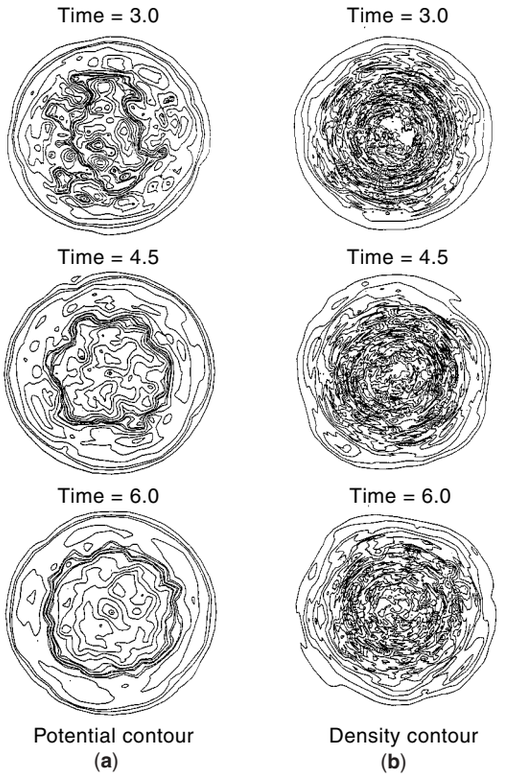

Figure 8. The evolution of (a) the electrostatic potential and (b) the density contours for the 3-D turbulence given by the resistive drift wave model with average unfavorable toroidal curvature. The time values are in units of (Courtesy of Wakatani).

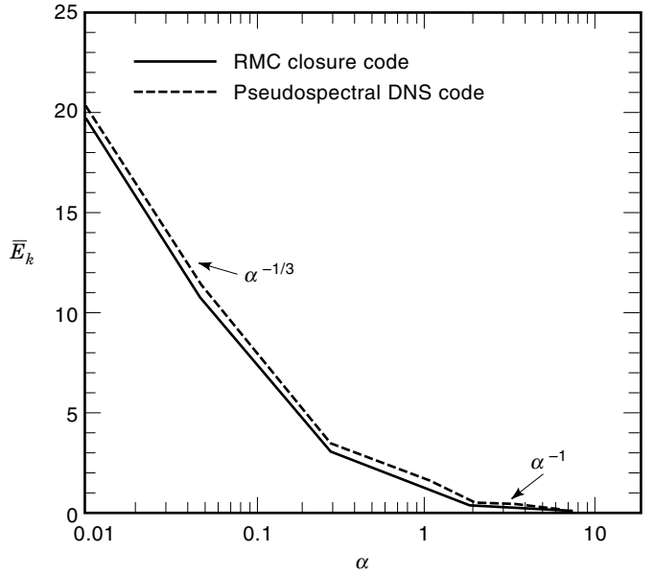

Figure 9. The power law decrease of the turbulent kinetic energy with adiabaticity parameter α in the Hasegawa–Wakatani equations. In the limit of large α the drift wave model reduces to the Terry–Horton model applicable at higher plasma temperatures.

trons tend to the Boltzmann distribution $\tilde{n} = e\phi/T_e$ and the Hasegawa–Mima equation is recovered. For intermediate values of $\alpha \gtrsim 1$ the Terry-Horton equation (64) applies.

Plasma turbulence appears as ubiquitous as plasma itself. Space, solar, and astrophysical plasmas show many varied forms of plasma turbulence ranging from large-scale magnetohydrodynamic (MHD) turbulence (65) to the smallest Debye length scale Langmuir turbulence. For example, the energy released during solar flares heats and accelerates the plasma in the solar corona. Electrons on the open coronal magnetic field lines caused by large-scale MHD reconnection events stream at relativistic speeds into the interplanetary plasma. The electron beams drive Langmuir turbulence creating intermittent bursts of radio noise known as type-III radio sources. The peculiar intermittency of Langmuir turbulence called nonlinear wave collapse was first described by Zakharov (66). The phenomenon of nonlinear wave collapse is reviewed by Robinson (67) in a wide range of laboratory and space physics settings. The general theoretical analysis of wave turbulence for plasmas and neutral fluids is given in Zakharov, L'vov, and Falkovich in *Kolmogorov Spectra of Turbulence* (68).

ACKNOWLEDGMENTS

The work was supported by the Department of Energy under Grant No. DE-FG03-96ER-54346.

BIBLIOGRAPHY

1. A. Taroni et al., Global and local energy confinement properties of simple transport coefficients of the Bohm type, *Plasma Phys. Contr. Fusion,* **36**: 1629–1646, 1994.
2. M. Erba et al., Extension of a Bohm model for L-mode electron heat transport to ion heat transport and to the ohmic regime, *Plasma Phys. Control. Fusion,* **37**: 1249–1261, 1995.
3. W. Horton, Nonlinear drift waves and transport in magnetized plasma, *Phys. Rep.,* **192**: 1, 1990.
4. W. Horton, R. Estes, and D. Biskamp, Fluid simulation of ion pressure gradient driven drift modes, *Plasmas Phys.,* **22**: 663–678, 1980.
5. M. Wakatani and A. Hasegawa, A collisional drift wave description of plasma edge turbulence, *Phys. Fluids,* **27**: 611, 1984.
6. M. C. Kelley and R. A. Heelis, *The Earth's Ionosphere, Plasma Physics and Electrodynamics,* San Diego, CA: Academic Press, 1989, Vol. 43.
7. O. Buneman, Instability, turbulence, and conductivity in a current-carrying plasma, *Phys. Rev. Lett.,* **10**: 285, 1963.
8. M. J. Keskinen, S. L. Ossakow, and P. K. Chaturvedi, *J. Geophys. Res.,* **85**: 3485, 1980.
9. R. N. Sudan, *Geophys. Res. Lett.,* **88**: 4853, 1983.
10. S. M. Hamberger and J. Jancarik, Experimental studies of electrostatic fluctuations in a turbulently heated plasma, *Phys. Fluids,* **15**: 825, 1972.
11. R. E. Slusher et al., Study of current-driven ion-acoustic instability using CO_2-laser scattering, *Phys. Rev. Lett.,* **36**: 674, 1976.
12. W. Horton, D.-I. Choi, and R. A. Koch, Ion acoustic heating from renormalized turbulence theory, *Phys. Rev. A,* **14**: 424, 1976.

12a. R. L. Stenzel, Experiment on current-driven three-dimensional ion sound turbulence, *Phys. Fluids,* **21**: 93, 99, 1978.

13. W. Horton and W. Rowan, Impurity transport studies in the Texas Experimental Tokamak (TEXT), *Phys. Plasmas,* **1**: 901–908, 1994.

14. H. W. Hendel, T. K. Chu, and P. A. Politzer, Collisional drift waves-identification, stabilization, and enhanced plasma x transport, *Phys. Fluids,* **11**: 2426–2439, 1968.

15. F. L. Hinton and W. Horton, Amplitude limitation of a collisional drift wave instability, *Phys. Fluids,* **14**: 116–123, 1971.

16. H. L. Pécseli, J. Juul Rasmussen, and K. Thomsen, Nonlinear interaction of convective cells in plasmas, *Phys. Rev. Lett.,* **52**: 2148–2151, 1984.

17. H. L. Pécseli, J. Juul Rasmussen, and K. Thomsen, Nonlinear interaction of convective cells in plasmas, *Plasma Phys. Contr. Fusion,* **27**: 837–846, 1985.

18. S. C. Prager, A. K. Sen, and T. C. Marshall, Dissipative trapped-electron instability in cylindrical geometry, *Phys. Rev. Lett.,* **33**: 692–695, 1974.

19. J. Slough, G. A. Navratil, and A. K. Sen, Production and observation of the dissipative trapped ion instability, *Phys. Rev. Lett.,* **47**: 1057, 1982.

20. R. Scarmozzino, A. K. Sen, and G. A. Navratil, Production and identification of a collisionless, curvature-driven, trapped-particle instability, *Phys. Rev. Lett.,* **57**: 1729–1732, 1986.

21. A. K. Sen, J. Chen, and M. Mauel, Production and identification of the ion-temperature-gradient instability, *Phys. Rev. Lett.,* **66**: 429–432, 1991.

22. J. Chen and A. K. Sen, Experimental study of a mixed slab and toroidal ion-temperature-gradient mode, *Phys. Plasmas,* **2**: 3063, 1995.

22a. T. Ohkawa and M. Yoshikawa, Experimental observation and theoretical interpretation of low-frequency interchange instability in "average minimum-B" configurations, *Phys. Rev. Lett.,* **19**: 1374, 1987.

23. M. Okabayashi and V. Arunasalam, Study of drift-wave turbulence by microwave scattering in a toroidal plasma, *Nucl. Fusion,* **17**: 497–513, 1977.

24. E. J. Synakowski et al., *Phys. Plasmas,* **4**: 1736–1744, 1997.

25. K. H. Burrell, Effects of $\mathbf{E} \times \mathbf{B}$ velocity shear and magnetic shear on turbulence and transport in magnetic confinement devices, *Phys. Plasmas,* **4**: 1499–1518, 1997.

26. Y. Koide et al., Internal transport barrier on $q = 3$ surface and poloidal plasma spin-up in JT-60U high-β_p discharges, *Phys. Rev. Lett.,* **72**: 3662–3665, 1994.

27. F. M. Levinton et al., Improved confinement with reversed magnetic shear in TFTR, *Phys. Rev. Lett.,* **75** (24): 4417–4420, 1995.

28. E. J. Strait et al., Enhanced confinement and stability in DIII-D discharges with reversed magnetic shear, *Phys. Rev. Lett.,* **75** (24): 4421, 1995.

29. E. Mazzucato, Small-scale density fluctuations in the adiabatic toroidal compressor, *Phys. Rev. Lett.,* **36**: 792–794, 1976.

30. C. M. Surko and R. E. Slusher, Study of the density fluctuations in the adiabatic toroidal compressor scattering Tokamak using CO_2 laser, *Phys. Rev. Lett.,* **36**: 1747–1750, 1976.

31. C. M. Surko and R. E. Slusher, Study of density fluctuations in the Alcator Tokamak using CO_2 laser scattering, *Phys. Rev. Lett.,* **40**: 400–403, 1978.

32. R. V. Bravenec et al., Core turbulence and transport studies on the Texas Experimental Tokamak, *Phys. Fluids B,* **4**: 2127–2135, 1992.

33. K. W. Gentle, Diagnostics of magnetically confined high-temperature plasma, *Rev. Mod. Phys.,* **67**: 80, 1995.

33a. E. Mazzucato et al., Turbulent fluctuation in TFTR configurations with reversed magnetic shear, *Phys. Rev. Lett.,* **77**: 3145, 1996.

34. H. Sugama et al., Transport processes and entropy production in toroidal plasma with gyrokinetic electromagnetic turbulence, *Phys. Plasmas,* **3**: 2379, 1996.

35. W. Horton and Y.-H. Ichikawa, *Chaos and Structures in Nonlinear Plasmas,* Singapore: World Scientific, 1996, pp. 234–317.

36. C. C. Petty et al., Gyroradius scaling of electron and ion transport, *Phys. Rev. Lett.,* **74**: 1763–1766, 1995.

37. T. Tajima et al., U.S.-Japan Workshop on "Ion Temperature Gradient-Driven Turbulent Transport," in *AIP Convergence Proceedings No. 284,* p. 255, 1994.

38. Y. Kishimoto et al., Theory of self-organized critical transport in tokamak plasmas, *Phys. Plasmas,* **3**: 1289–1307, 1996.

39. Y. Kishimoto et al., Self-organized critical gradient transport and shear flow effects for the ion temperature gradient mode in toroidal plasmas, *Plasma Physics and Controlled Nuclear Fusion Research, 1994* (International Atomic Energy Agency, Vienna: 1996), vol. 3, pp. 299–307.

40. X. Garbet and R. E. Waltz, Action at distance and Bohm scaling of turbulence in tokamaks, *Phys. Plasmas,* **3**: 1898–1907, 1996.

41. J. W. Connor and H. R. Wilson, Survey of theories of anomalous transport, *Plasma Phys. Control. Fusion,* **36**: 719, 1994.

42. S. E. Parker et al., Radially global gyrokinetic simulation studies of transport barriers, *Phys. Plasmas,* **3**: 1959–1966, 1996.

43. R. D. Sydora, V. K. Decyk, and J. M. Dawson, Fluctuation-induced heat transport results from a large global 3D toroidal particle simulation model, *Plasma Phys. Control. Fusion A,* **38**: 281, 1996.

44. R. E. Waltz, J. C. DeBoo, and M. N. Rosenbluth, Magnetic-field scaling of dimensionally similar tokamak discharge, *Phys. Rev. Lett.,* **65**: 2390, 1990.

45. F. Perkins et al., Nondimensional transport scaling in the Tokamak Fusion Test Reactor: Is tokamak transport Bohm or gyro-Bohm?, *Phys. Fluids B,* **5**: 477–498, 1993.

46. E. J. Doyle et al., Modifications in turbulence and edge electric fields at the L-H transition in the DIII-D tokamak, *Phys. Fluids B,* **3**: 2300–2307, 1991.

47. E. Mazzucato and R. Nazikian, Radial scale length of turbulent fluctuations in the main core of TFTR plasmas, *Phys. Rev. Lett.,* **71**: 1840–1843, 1993.

48. R. D. Durst et al., Observation of a localized transition from edge to core density turbulence in the TFTR tokamak, *Phys. Rev. Lett.,* **71**: 3135–3138, 1993.

49. D. L. Brower, W. A. Peebles, and N. C. Luhmann, Jr., Multichannel scattering studies of the spectra and spatial distribution of Tokamak microturbulence, *Phys. Rev. Lett.,* **54**: 689–692, 1985.

50. D. L. Brower et al., Observation of a high-density ion mode in tokamak microturbulence, *Phys. Rev. Lett.,* **59**: 48, 1987.

51. A. Hasegawa and K. Mima, Stationary spectrum of strong turbulence in magnetized plasma, *Phys. Rev. Lett.,* **39**: 205, 1977.

52. A. Hasegawa and K. Mima, Pseudo-three-dimensional turbulence in magnetized nonuniform plasma, *Phys. Fluids,* **21**: 87–92, 1978.

53. A. Hasegawa, C. G. MacLennan, and Y. Kodama, Nonlinear behavior and turbulence spectra of drift waves and Rossby waves, *Phys. Fluids,* **22**: 2122–2129, 1979.

54. V. I. Petviashvili, Self-focusing of an electrostatic drift wave, *Fiz. Plazmy,* **3**: 270 (*Sov. J. Plasma Phys.,* **3**: 150), 1977.

55. S. V. Antipov et al., Rossby soliton in the laboratory, *Zh. Eskp. Teor. Fiz.,* **82**: 145–160, 1982 (*Sov. Phys. JETP,* **55**: 85, 1982).

56. S. V. Antipov et al., Rossby autosoliton and laboratory model of Jupiter's Great Red Spot, *Sov. Phys. JETP,* **62**: 1097, 1985.

57. R. A. Antonova et al., Drift solitons in a shallow rotating fluid, *Pisma Zh. Eksp. Teor. Fiz.,* **37**: 545, 1983 (*JETP Lett.,* **37**: 651, 1983).

58. W. Horton and A. Hasegawa, Quasi-two-dimensional dynamics of plasmas and fluids, *CHAOS,* **4**: 227–251, 1994.

58a. S. Hamaguchi and W. Horton, *Phys. Fluids,* **B2**: 1833, 1990.

58b. G. W. Hammett, W. Dorland, and F. W. Perkins, *Phys. Fluids,* **B4**: 2052, 1992.

58c. M. Kotschereuther et al., *Phys. Plasmas,* **2**: 2381, 1995.

59. R. E. Waltz, G. D. Kerbel, and J. Milovich, Toroidal gyro-Landau fluid model turbulence simulations in a nonlinear ballooning mode representation with radial modes, *Phys. Plasmas,* **1**: 2229, 1994.

59a. R. E. Waltz et al., *Phys. Plasmas,* **2**: 2408, 1994.

59b. G. Rewoldt and W. M. Tang, *Phys. Fluids,* **B2**: 318, 1990.

59c. W. Horton, D.-I. Choi, and W. M. Tang, *Phys. Fluids,* **24**: 1077, 1981.

60. C. S. Chang and F. L. Hinton, Effect of impurity particles on the finite-aspect ratio neoclassical ion thermal conductivity in a tokamak, *Phys. Fluids,* **29**: 3314–3316, 1986.

60a. S. P. Hirshman and D. J. Sigmar, Neoclassical transport of impurities in tokamak plasmas, *Nucl. Fusion,* **21**: 1079, 1981.

60b. C. Bolton and A. A. Ware, *Phys. Fluids,* **26**: 459, 1983.

60c. H. Sugama and W. Horton, *Phys. Plasmas,* **2**: 2989, 1995.

60d. H. Sugama and W. Horton, *Phys. Plasmas,* **4**: 405, 1997.

60e. W. Horton et al., *Plasma Phys. Control. Fusion,* **39**: 83, 1997.

61. A. Hasegawa and M. Wakatani, Self-organization of electrostatic turbulence in a cylindrical plasma, *Phys. Rev. Lett.,* **59**: 1581–1584, 1987.

61a. J. A. Krommes and G. Hu, *Phys. Plasmas,* **1**: 3211, 1994.

61b. G. Hu, J. A. Krommes, and J. C. Bowman, *Phys. Plasmas,* **1**: 3211, 1996.

62. B. A. Carreras, L. Garcia, and P. H. Diamond, Theory of resistive pressure-gradient driven turbulence, *Phys. Fluids,* **30**: 1338, 1987.

63. M. Wakatani et al., Resistive drift wave and interchange turbulence in a cylindrical plasma with magnetic and velocity shear, *Phys. Fluids B,* **4**: 1754–1765, 1992.

64. P. W. Terry and W. Horton, Drift wave turbulence in a low-order k space, *Phys. Fluids,* **26**: 106–112, 1983.

65. D. Biskamp, *Nonlinear Magnetohydrodynamics,* Cambridge Univ. Press, 1997, Chaps. 7–10.

66. V. E. Zakharov, *Zh. Eksp. Teor. Fiz.,* **62**: 1745, 1972 (*Soviet Phys. JETP,* **35**: 908, 1972).

67. P. A. Robinson, Nonlinear wave collapse and strong turbulence, *Rev. Mod. Phys.,* 507–574, 1997.

68. V. E. Zakharov, V. S. L'vov, and G. Falkovich, *Kolmogorov Spectral of Turbulence,* New York: Springer-Verlag, 1992.

Reading List

H. L. Berk, D. D. Ryutov, and Yu. A. Tsidulko, Temperature-gradient instability induced by conducting end walls, *Phys. Fluids B,* **3**: 1346–1354, 1991.

J. W. Connor and H. R. Wilson, *Plasma Phys. Controlled Fusion,* **36**: 719, 1994.

A. Hasegawa and M. Wakatani, *Phys. Rev. Lett.,* **50**: 682, 1983.

W. Horton, M. Wakatani, and A. J. Wootton, Ion temperature gradient driven turbulent transport, *American Institute Physics Conf. Proc. No. 284,* New York, 1994.

B. B. Kadomtsev, *Plasma Turbulence,* New York: Academic Press, 1965, p. 68.

B. B. Kadomtsev and O. P. Pogutse, Trapped particles in toroidal magnetic systems, *Nucl. Fusion,* **11**: 67–92, 1971.

M. Ottaviani, W. Horton, and M. Erba, The long wavelength behaviour of ion-temperature-gradient-driven turbulence and the radial dependence of the turbulent ion conductivity, *Plasma Phys. Contr. Fusion,* **39**: 1461–1477, 1997.

C. C. Petty et al., Nondimensional transport scaling in DIII-D: Bohm versus gyro-Bohm resolved, *Phys. Plasmas,* **2**: 2342–2348, 1995.

W. HORTON
The University of Texas
G. HU
Globalstar LP

PLASTIC PACKAGINGS. See ENCAPSULATION MATERIALS AND PROCESSES.

PLATFORMS FOR MOBILE ROBOTS. See MOBILE ROBOTS.

PLLS. See PHASE LOCKED LOOPS.

PN MODELS. See PETRI NETS.

POLARIMETRY, RADAR. See RADAR POLARIMETRY.

POLLUTION, FROM POWER PLANTS. See AIR POLLUTION CONTROL.

POLYCRYSTALLINE THIN FILM SOLAR CELLS. See TERNARY SEMICONDUCTORS.

POLYNOMIAL EQUATIONS. See POLYNOMIALS.